Molecules and Cells

Crystal Structure of LysB4, an Endolysin from *Bacillus cereus*-Targeting Bacteriophage B4

Seokho Hong[1,2], Bokyung Son[1,2], Sangryeol Ryu[1,*], and Nam-Chul Ha[1,*]

[1]Department of Agricultural Biotechnology, Research Institute of Agriculture and Life Sciences, Center for Food and Bioconvergence, Center for Food Safety and Toxicology, Seoul National University, Seoul 08826, Korea, [2]These authors contributed equally to this work.
*Correspondence: sangryu@snu.ac.kr (SR); hanc210@snu.ac.kr (NCH)
http://dx.doi.org/10.14348/molcells.2018.0379
www.molcells.org

Endolysins are bacteriophage-derived enzymes that hydrolyze the peptidoglycan of host bacteria. Endolysins are considered to be promising tools for the control of pathogenic bacteria. LysB4 is an endolysin produced by *Bacillus cereus*-infecting bacteriophage B4, and consists of an N-terminal enzymatic active domain (EAD) and a C-terminal cell wall binding domain (CBD). LysB4 was discovered for the first time as an L-alanoyl-D-glutamate endopeptidase with the ability to breakdown the peptidoglycan among *B. cereus*-infecting phages. To understand the activity of LysB4 at the molecular level, this study determined the X-ray crystal structure of the LysB4 EAD, using the full-length LysB4 endolysin. The LysB4 EAD has an active site that is typical of LAS-type enzymes, where Zn^{2+} is tetrahedrally coordinated by three amino acid residues and one water molecule. Mutational studies identified essential residues that are involved in lytic activity. Based on the structural and biochemical information about LysB4, we suggest a ligand-docking model and a putative endopeptidase mechanism for the LysB4 EAD. These suggestions add insight into the molecular mechanism of the endolysin LysB4 in *B. cereus*-infecting phages.

Keywords: *Bacillus cereus*, bacteriophage B4, endolysin, LAS-type enzyme, L-alanoyl D-glutamate endopeptidase

INTRODUCTION

Endolysins are peptidoglycan hydrolases produced by bacteriophages at the end of their replication cycles to breakdown the peptidoglycan of host bacteria (Schmelcher et al., 2012). Endolysins have been considered to be one of the most promising phage products for controlling antibiotic-resistant bacteria since they have narrow host specificity, high sensitivity, and there is a low probability for the development of bacterial resistance (Borysowski et al., 2006). In general, the endolysins from phages infecting Gram-positive bacteria commonly consist of two distinct domains: an N-terminal enzymatic active domain (EAD) that is responsible for the hydrolysis of peptidoglycans, and a C-terminal cell wall binding domain (CBD) that confers enzymatic specificity to endolysins by anchoring to cell wall components (Loessner, 2005; Nelson et al., 2012). These endolysin features suggest their potential as antimicrobial and detection agents.

Endolysin LysB4 was identified in the genome of *Bacillus cereus*-infecting phage B4 (Lee et al., 2013) and exhibited the enzymatic activity of an L-alanoyl-D-glutamate endopeptidase on peptidoglycans (Son et al., 2012). LysB4 was predicted to consist of a VanY domain as an EAD and a SH3_5 domain as a CBD, according to InterProScan analysis (http://

Received 20 September 2018; revised 30 October 2018; accepted 11 November 2018; published online 5 December, 2018

eISSN: 0219-1032

www.ebi.ac.uk/Tools/pfa/iprscan/)(Jones et al., 2014). *In silico* analysis of the amino acid sequence of LysB4 indicates that its EAD is highly similar to that of Ply500, an endolysin of *Listeria* phage A500, and CwlK, which is encoded in *B. subtilis* (Fukushima et al., 2007; Loessner et al., 1995). Crystal structure of the EAD of Ply500 from the *Listeria* bacteriophage A500 has been determined and revealed that it belongs to a family of Zn^{2+}-dependent peptidases of the lysostaphin-type, D-Ala-D-Ala metallopeptidases, and the sonic hedgehog (LAS) family (Korndorfer et al., 2008). Most endolysins from *Bacillus*-infecting phages were predicted to be amidases. However, LysB4 exhibited endopeptidase activity, together with PlyP56, which was recently discovered (Etobayeva et al., 2018). Thus, further study is required on the endopeptidases from *B. cereus* phages to understand the breakdown stage for bacteriophages infecting *Bacillus*.

In the previous study, LysB4 exhibited antimicrobial activity against Gram-positive bacteria such as *Listeria monocytogenes*, *B. cereus*, and *B. subtilis*. Moreover, this enzyme also showed lytic activity against all tested Gram-negative bacteria when the outer membrane was disrupted (Son et al., 2012). Since the bacteria tested contained so-called DAP-type peptidoglycans (Kamisango et al., 1982; Schleifer and Kandler, 1972), LysB4 was suggested to work on the DAP-type peptidoglycan. However, LysB4 failed to hydrolyze a certain group of Gram-positive bacteria, such as *Enterococcus faecalis*, *Staphylococcus aureus*, *Lactococcus lactis*, and *Streptococcus thermophiles*, which contain the lysine-type peptidoglycan (Schleifer and Kandler, 1972; Son et al., 2012; Vollmer et al., 2008). Therefore, the previous study concluded that LysB4 preferentially cleaves a peptide bond between L-alanine and D-glutamic acid of the DAP-type peptidoglycan over the lysine-type peptidoglycan (Son et al., 2012).

Here, we determined the X-ray crystal structure of the LysB4 EAD, using the full-length LysB4 endolysin, to reveal the working mechanism of the endolysin based on the high resolution structure. The ensuing studies give molecular insights into the function of the LysB4 of *B. cereus*-infecting phages, which was discovered for the first time as the L-alanoyl-D-glutamate endopeptidase from *B. cereus*-infecting phages.

MATERIALS AND METHODS

Protein expression and purification

Construction of the recombinant plasmid encoding LysB4 endolysin was described previously (Son et al., 2012). Briefly, the *lysB4* gene was amplified from the genomic DNA of the bacteriophage B4 by polymerase chain reaction (PCR), and the PCR product was inserted into pET15b vector (Novagen, USA). The recombinant plasmid was transformed into *E. coli* BL21 (DE3) competent cells. The cells were grown in 1.6 L of Luria-Bertani (LB) medium (Merck, USA) supplemented with 100 μg/ml ampicillin at 37℃ until the OD_{600} reached ~0.7 and induced with 0.1 mM isopropyl β-D-1-thio-galactopyranoside (IPTG) at 30℃ for 6 h. The cells were harvested by centrifugation at 5,000 x g for 7 min and resuspended with 50 ml lysis buffer containing 20 mM Tris-HCl (pH 8.0), 150 mM NaCl, and 2 mM β-mercaptoethanol. The cell lysate was disrupted by sonication and centrifuged at 10,000 x g to remove cell debris. The supernatant was loaded onto an open column packed with Ni-NTA affinity resin (GE Healthcare, USA). The resin was washed with 400 ml lysis buffer supplemented with 20 mM imidazole. After washing the resin, the protein was eluted with 30 ml lysis buffer supplemented with 250 mM imidazole. Eluted recombinant proteins were loaded on size exclusion chromatography using a Superdex 200 HiLoad 26/600 column (GE Healthcare, USA) pre-equilibrated with the lysis buffer. The final purified samples was concentrated to 18 mg/ml using a Vivaspin® centrifugal concentrator with 30 kDa cutoff (Sartorius, Germany) and stored frozen at - 80℃ until use.

Crystallization and data collection

A single crystal of LysB4 was obtained by the hanging-drop vapor diffusion method using a precipitant solution consisting of 2.0 M ammonium sulfate, 0.1 M Bis-Tris pH 6.5, 2% polyethylene glycol monomethyl ether 550 (PEG MME 550), and 8 mM Tris (2-carboxyethyl) phosphine (TCEP). Equal volumes (1 μl) of the protein and reservoir solution were mixed and equilibrated against 500 μl reservoir solution at 14℃ for two weeks. The crystals were dehydrated by adding excess amount of ammonium sulfate into the reservoir solution and were then flash-cooled in a liquid nitrogen stream at -173℃ (Jang et al., 2018). A native X-ray diffraction data set and a single-wavelength anomalous data set were collected on beamlines 5C and 7A at Pohang Accelerator Laboratory (PAL) (Pohang, Republic of Korea).

Structural determination and refinement

X-ray diffraction data were processed using HKL2000 software (Otwinowski and Minor, 1997). The structure of LysB4 was determined by the molecular replacement method with MOLREP (Vagin and Teplyakov, 2010) in the CCP4 package (Winn et al., 2011) using the structure of Ply500 EAD (PDB code: 2VO9) as a search model (Korndorfer et al., 2008). The position of Zn^{2+} was determined by zinc single-wavelength anomalous dispersion (Zn-SAD) phasing with Phaser software (McCoy et al., 2007) and the final structure of LysB4 was refined using the PHENIX software suite (Adams et al., 2010).

Ligand docking

A ligand was generated with the Restraint Editor Especially Ligands (REEL) program in the PHENIX software suite (Adams et al., 2010) and manually docked and adjusted in the LysB4 EAD with Coot software (Emsley et al., 2010). The complex structure of the LysB4 EAD and the ligand was further refined using Phenix.refine program in the PHENIX software suite with energy optimization option (weight of X-ray data/stereochemistry was set to 0) (Adams et al., 2010).

Strains, media, and culture conditions

All bacterial strains for the endopeptidase activity assay are listed in Table 2 and were routinely grown in LB broth medium at 37℃ with aeration. *E. coli* DH5α and BL21 (DE3) strains were used for cloning and expression of endolysins, respectively.

Construction of LysB4 mutants

The K15Q, R50Q, R74T, and D129A mutants of LysB4 were constructed via an overlapping extension PCR protocol (Nelson and Fitch, 2012). To construct pET15b_LysB4 K15Q, the *lysB4* gene was amplified from the pET15b_LysB4 vector in two parts, using two sets of primers (BglII-pET15b-F and lysB4-K15Q-R for the front part; lysB4-K15Q-F and lysB4-BamHI-R for the rear part). Two overlapping PCR fragments containing the single mutation were used for the second PCR step generating the *lysB4* (K15Q) gene. The resultant PCR product was inserted between the NdeI/BamHI restriction sites of pET15b to construct lysB4 K15Q-containing pET15b (pET15b_LysB4 K15Q). For the construction of pET15b_LysB4 R50Q, pET15b_LysB4 R74T, and pET15b_LysB4 D129A, two corresponding sets of primers were used. The sequences of primers used in this study are listed in the supporting information Supplementary Table S1.

Circular dichroism

Circular dichroism (CD) spectra of LysB4, LysB4 R50Q, and LysB4 D129A (1 mg/ml) in the reaction buffer (50 mM Tris-HCl, pH 8.0) were measured using Chirascan™-plus CD Spectrometer (Applied Photophysics, Leatherhead, United Kingdom) at NICEM in Seoul National University (Seoul, Republic of Korea). The spectra were recorded over 190-260 nm range using a cuvette with the optical path length of 0.2 mm.

Endopeptidase activity assay

The endopeptidase activity of LysB4 and its mutants (LysB4 K15Q, R50Q, R74T, and D129A) was evaluated against bacterial cells by monitoring the decrease in OD_{600}. All tested bacteria were cultivated to the exponential phase. Cells were harvested and resuspended with reaction buffer (50 mM Tris-HCl, pH 8.0) to an OD_{600} of 0.8-1.0. In the case of Gram-negative bacteria, exponentially growing cells were pretreated with a reaction buffer containing 0.1 M EDTA for 5 min at 25℃, and the cells were washed three times with reaction buffer to remove residual EDTA, as previously described (Leive, 1968). Endolysins (300 nM in final concentration, 100 μl) were added to the cell suspension (900 μl) followed by incubation at 25℃, unless indicated otherwise. OD_{600} values were monitored over time.

RESULTS

The crystal structure of LysB4

We overexpressed the full-length LysB4 endolysin in the *E. coli* expression system and purified the protein successfully. The protein was crystalized at pH 6.5 in the intact form (~32

Table 1. X-ray diffraction and refinement statistics

	LysB4	LyaB4 (Zn-SAD)
Data collection		
Beam line	PAL 7A	PAL 5C
Wavelength (Å)	0.97934	1.28250
Space group	$I4_1$	$I4_1$
Cell dimensions		
a, *b*, *c* (Å)	79.46, 79.46, 77.93	80.42, 80.42, 78.16
α, β, γ (°)	90.0, 90.0, 90.0	90.0, 90.0, 90.0
Resolution (Å)	50.0-2.40 (2.44-2.40)	50.0-2.67 (2.72-2.67)
R_{merge}	0.057 (0.351)	0.095 (0.412)
$I/\sigma I$	19.66 (2.36)	18.94 (2.61)
Completeness (%)	91.5 (92.4)	99.1 (90.4)
Redundancy	4.9 (2.9)	6.6 (3.4)
Refinement		
Resolution (Å)	28.1-2.40	
No. reflections	7926	
R_{work}/R_{free}	0.181/0.224	
No. of Total atoms	1190	
Wilson B-factor (Å)	32.75	
R.M.S deviations		
Bond lengths (Å)	0.007	
Bond angles (°)	0.785	
Ramachandran plot		
Favored (%)	94.6	
Allowed (%)	5.4	
Outliers (%)	0	
PDB ID	6AKV	

kDa), as confirmed by sodium dodecyl sulfate-polyacrylamide gel electrophoresis (SDS-PAGE) analysis of a dissolved crystal sample (Supplementary Fig. S1). The cell content analysis using Phenix.xtriage (Adams et al., 2010) suggested one copy of LysB4 per asymmetric unit with a 41.1% solvent content and 2.09 Å^3/Da Matthews coefficient. The crystal structure of LysB4 was determined at 2.38 Å resolution in the space group of $I4_1$ via the molecular replacement method using the structure of Ply500 EAD (PDB code: 2VO9) as a search model (Korndorfer et al., 2008)(Table 1).

One molecule was contained in the asymmetric unit of the crystal as predicted. The N-terminal EAD was well ordered in the crystal. Unfortunately, the C-terminal CBD was completely disordered in the solvent channel of the crystal because of a flexible linker (GGSGSTGGSGGGSTGGGSTGG; 156-176 amino acids) between the EAD and the CBD. Thus, we were able to obtain the structural information of only the EAD of LysB4 in this crystal structure. Our findings further suggest that a direct contact between the EAD and the CBD is unlikely. One zinc ion and a sulfate molecule were also found in the structure. The presence of Zn^{2+} was confirmed by single-wavelength anomalous signal with X-ray absorption edges of Zn^{2+} (Fig. 1).

The LysB4 EAD (1-152) consists of five α-helices and one β-sheet containing three antiparallel β-strands (β1, β2, and β3)(Fig. 1A). A subdomain was composed of the β-sheet with three helices (α1, α2, and α5), and the other two helices (α3 and α4) make a flap from the subdomain, forming a deep cleft between them. The flap also contains a long loop linking α3 and α4, which appears to provide structural flexibility to the flap against the subdomain (Fig. 1A). The Zn^{2+} was tetrahedrally coordinated by His80 from α4, Asp87 from β2, His132 from β3, and one water molecule in the cleft region (Fig. 1B). The sulfate ion, which was contained in the crystal precipitant solution, was bound in the cleft near the Zn^{2+} (Fig. 1B).

Structural comparison to Ply500 EAD

The overall shape of the LysB4 EAD is similar to the structure of Ply500 EAD (PDB code: 2VO9), whose crystal was obtained using a truncated endolysin protein containing only the EAD (Korndorfer et al., 2008)(Fig. 2A). Ply500 EAD has an amino acid sequence identity of 71% relative to the LysB4 EAD. Both EAD seem to show the similar enzymatic activities even though the activity of Ply500 EAD was not tested on the Gram-negative bacteria. Structural superposition with two EAD structures reveals that the overall structures of the two proteins are very similar (rmsd = 0.457 Å over 120 atoms; 8-92, 95-100, 108-124, 129-139, and 142 amino acids) with a variation in the conformation of a C-terminal loop of the LysB4 EAD. More amino acids were ordered in the loop of LysB4 from the bacteriophage B4 than the C-terminal amino acid sequence of Ply500 EAD from the bacteriophage A500 (Fig. 2A). Although the bacteriophages B4 and A500 exhibit different host bacteria, LysB4 and Ply500 exhibited the same L-alanoyl-D-glutamate endopeptidase activity with a bound Zn^{2+} coordinated by two histidines and an aspartate (Korndorfer et al., 2008).

The Zn^{2+} was further coordinated by a bound water molecule in the LysB4 EAD, as observed in the typical LAS-type enzymes containing the SxHxxGxAxD motif (Bochtler et al., 2004; Bussiere et al., 1998; McCafferty et al., 1997). The

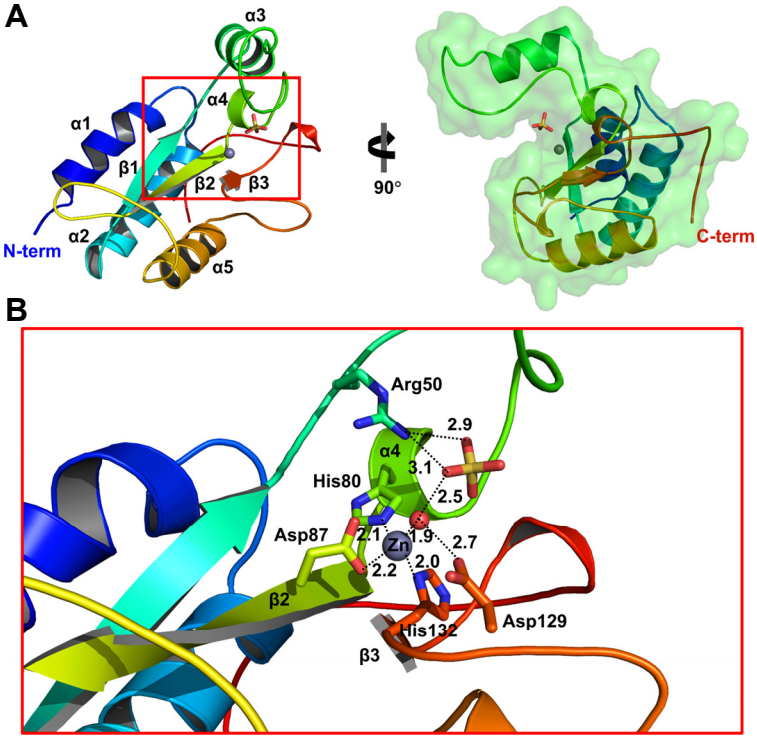

Fig. 1. The structure of the LysB4 EAD. (A) The overall structure of the LysB4 EAD, consisting of five α-helices and one β-sheet with three antiparallel β-strands (the blue to red ribbon model in the *left* and the green transparent surface model in the *right*). Zn^{2+} is represented as the gray sphere, and a sulfate ion in the cleft is shown in the stick model. (B) A close-up view of the red inset in A. The Zn^{2+} (gray sphere) shows the tetrahedral coordination geometry with His80 from α4, Asp87 from β2, His132 from β3, and one water molecule (red sphere) in the cleft region. The adjacent sulfate ion is shown in the stick model and makes polar interactions with Arg50 and the bound water molecule. The distances are indicated by a dotted line (Å).

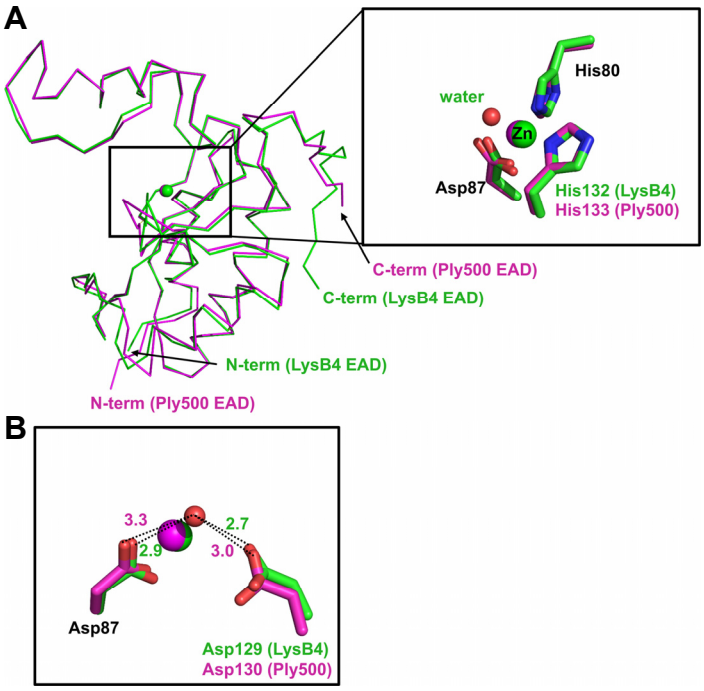

Fig. 2. Structural comparison to Ply500 EAD. (A) The LysB4 EAD and Ply500 EAD (PDB code: 2VO9) are displayed in the ribbon model (green and magenta, respectively). Zn^{2+} is in the ball representation, and a water molecule (red sphere), shown in the inset, is from the LysB4 EAD model. (B) Structural comparison of the (putative) water binding environments. The distances in Ply500 EAD were measured based on the location of the water molecule within the LysB4 EAD.

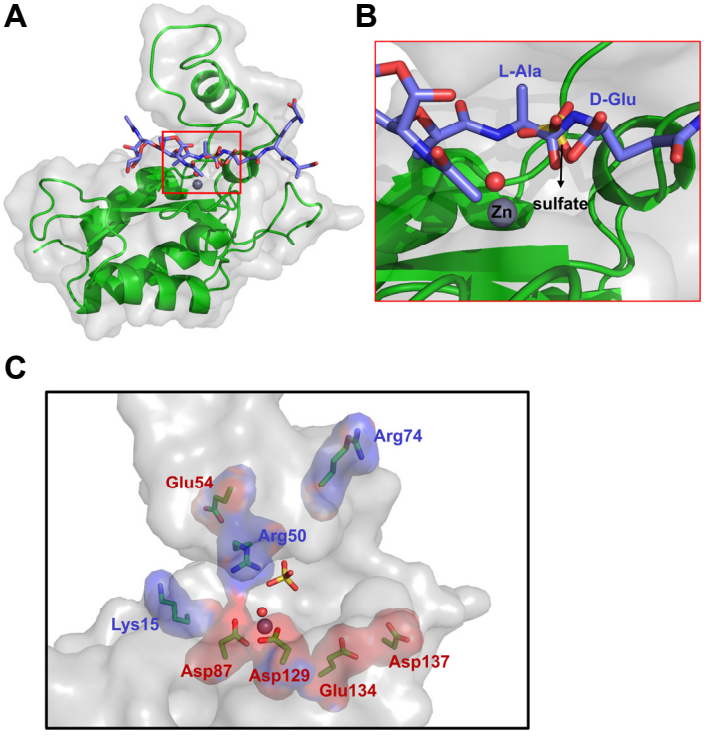

Fig. 3. Ligand docking model with Glc*N*Ac-Mur*N*Ac-L-Ala-D-Glu-*meso*-DAP-D-Ala. (A) The docking model of the LysB4 EAD with the ligand (Glc*N*Ac-Mur*N*Ac-L-Ala-D-Glu-*meso*-DAP-D-Ala). The LysB4 EAD is shown in the cartoon (green) and surface (gray) representation, and the ligand is shown in the stick model (purple). (B) The carbonyl group of the peptide linkage between L-alanine and D-glutamic acid overlaps with the site of the sulfate ion. The sulfate ion is shown in the stick model (yellow) and the bound water molecule and Zn^{2+} are shown in a red sphere and a gray sphere, respectively. (C) The basic residues (blue) and acidic residues (red) of the LysB4 EAD around the active cleft. Zn^{2+} (gray sphere), the water molecule (red sphere), and the sulfate ion (yellow stick model) in the cleft are shown.

water molecule further interacts with the side chains of Asp87 and Asp129 (2.9 Å and 2.7 Å, respectively; Fig. 2B). Interestingly, the bound water molecule was not observed in the structure of Ply500 EAD (Korndorfer et al., 2008), which indicates a weaker affinity for the water molecule in Ply500 EAD. The weaker affinity of the water molecules might result from the increased distances with the corresponding Asp residues (Asp87 and Asp130) involved in the water binding (3.3 Å and 3.0 Å, respectively; Fig. 2B).

Table 2. Endopeptidase activity assay against several bacteria

Organisms		Relative lytic activity				
		LysB4	LysB4 (R50Q)	LysB4 (D129A)	LysB4 (K15Q)	LysB4 (R74T)
Gram-negative bacteria	*Escherichia coli* MG1655	+	-	-	+	+
	Pseudomonas aeruginosa ATCC 27853	+	-	-	+	+
	Cronobacter sakazakii ATCC 29544	+	-	-	+	+
	Shigella flexineri 2a strain 2457T	+	-	-	+	+
	Salmonella Typhimurium LT2	+	-	-	+	+
Gram-positive bacteria	*Listeria monocytogenes* ATCC19114	+	-	-	+	+
	Bacillus cereus KCCM 40133	+	-	-	+	+
	Bacillus subtilis 168	+	-	-	+	+
	Enterococcus faecalis ATCC29212	-	-	-	-	-
	Staphylococcus aureus ATCC 29213	-	-	-	-	-
	Streptococcus thermophilus ATCC 19258	-	-	-	-	-

*+, positive activity; -, negative activity

Ligand docking model of the LysB4 EAD

To gain insight into the molecular basis for the substrate specificity of LysB4 toward the DAP-type peptidoglycan, a ligand docking model was constructed with Glc*N*Ac-Mur*N*Ac-L-Ala-D-Glu-*meso*-DAP-D-Ala, which is the stem peptide of the DAP-type peptidoglycan. The sulfate ion is bound adjacent to the active water molecule coordinating Zn^{2+} and is geometrically similar to the tetrahedral intermediate of the sessile peptide bond, which led us to hypothesize that the bound sulfate ion is in the site of the tetrahedral intermediate of the cleaved peptide bond between the L-alanine and the D-glutamic acid in the enzymatic reaction. We also noted that the Trp100 residue at the outer edge of the cleft is within a distance to make an interaction with a pyranose ring of sugar. It is generally known that the aromatic ring of tryptophan residue can interact with a sugar pyranose ring of Glc*N*Ac (Asensio et al., 2013). Combining these findings, we manually docked the ligand peptide into the deep cleft of the LysB4 EAD (Fig. 3A). The aromatic ring of the Trp100 residue made a π-interaction with the pyranose ring of Glc*N*Ac, and the carbonyl group of the peptide bond between L-alanine and D-glutamic acid was located in the position of the sulfate ion (Fig. 3B). However, the high resolution structure of the complex with the stem peptide is required to elucidate the substrate binding mode.

A putative mechanism of LysB4 endopeptidase activity

According to the results from VanX, Glu181 acts as a general base to deprotonate the bound water molecule coordinating Zn^{2+} in the cleft (Bussiere et al., 1998). The studies on ChiX also suggest that the water molecule is deprotonated by Zn^{2+} and the acidic residue that interacts with the water molecule, and then the deprotonated water molecule attacks the carbonyl group of the peptide bond (Owen et al., 2018). To see if Asp129, which corresponds to VanX Glu181 and ChiX Asp120, plays the same role in catalysis, we measured the antimicrobial activity of the D129A mutant LysB4. As shown in Table 2, the mutation abolished the antimicrobial activity.

The Arg50 residue, which interacts with the bound sulfate ion (Fig. 1B), was next to be investigated. The corresponding Arg71 residue in VanX played an essential role in stabilization of the oxyanion during the catalysis steps (Bussiere et al., 1998). We produced the R50Q mutant protein and confirmed that the mutation abolished the activity of LysB4 in the digestion of peptidoglycan. Thus, our results indicate that LysB4 shares its catalytic mechanism with VanX. The correct folding of the mutant proteins was confirmed by the circular dichroism (CD) spectra (Fig. 4A). Based on these findings, we propose a catalytic mechanism for LysB4 (Fig. 4B). The water molecule bound by Zn^{2+} and Asp129 is deprotonated and makes a nucleophilic attack on the substrate's carbonyl group between L-alanine and D-glutamic acid. The negative charge of the tetrahedral intermediate is stabilized by Arg50.

DISCUSSION

Peptidoglycan recognition proteins (PGRPs) trigger immune responses in invertebrates by differentially recognizing peptidoglycans from Gram-negative and -positive bacteria (Dziarski and Gupta, 2006). PGRP-LE specifically recognizes the DAP-type peptidoglycan through the ionic interactions between a conserved arginine residue in the central cleft and the carboxylic group of *meso*-DAP (Lim et al., 2006). How could LysB4 distinguish the DAP-type peptidoglycan from the other types of peptidoglycans? We noted the three basic residues (Lys15, Arg50, and Arg74) in the active site cleft that play a role in recognizing the negatively charged *meso*-DAP. We showed that the Arg50 is critical in the catalysis of LysB4 (Table 2). However, it is unlikely that Arg50 is directly involved in the recognition of *meso*-DAP, since the Arg50 residue is too far from the carboxylic group of *meso*-DAP in the peptidoglycan in the docking model. We next tested the roles of Lys15 and Arg74 that are located at both ends of the active site cleft (Fig. 3C). The mutant LysB4 proteins (K15Q and R74T) were constructed and their antimicrobial activities were measured. As a result, the mutations did not

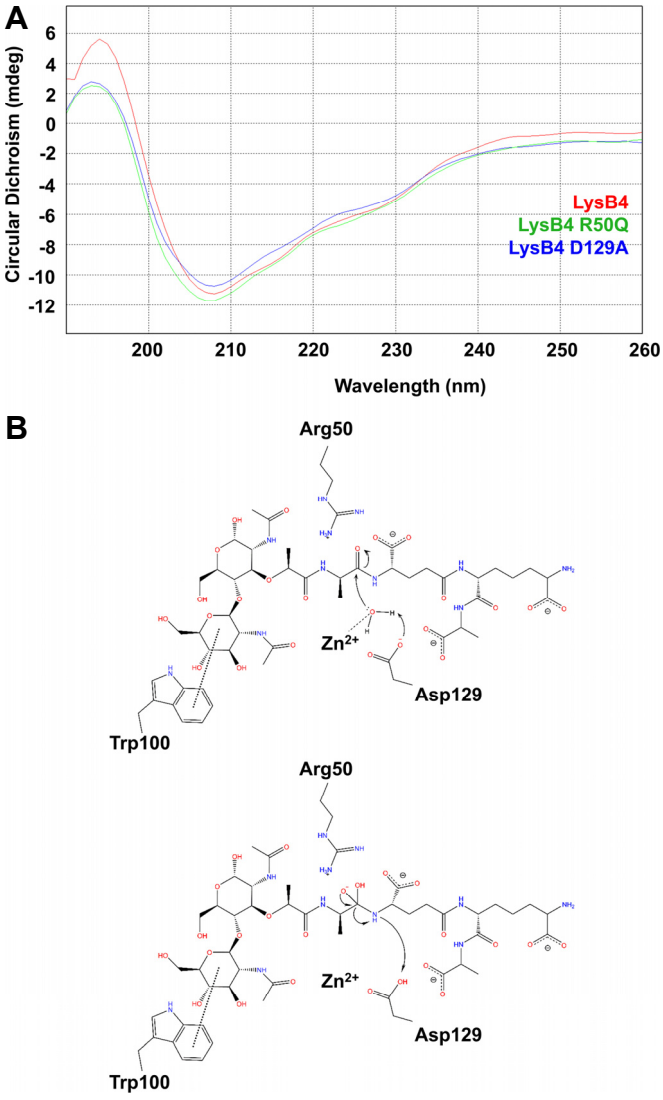

Fig. 4. The CD profiles and a putative endopeptidase mechanism of LysB4. (A). The circular dichroism (CD) profiles of the wild type LysB4 (red), LysB4 R50Q (green), and LysB4 D129A (blue). (B). One water molecule coordinating Zn^{2+} is deprotonated by Asp129 residue (*top*). Then, the deprotonated water executes a nucleophilic attack on a carbonyl carbon of the peptide bond between L-alanine and D-glutamic acid in peptidoglycan stem peptide (*top*). In the next intermediate step, the Arg50 residue stabilizes the negatively charged tetrahedral intermediate (*bottom*).

affect antimicrobial activity. Thus, our findings suggest that the three basic residues might not play a crucial role in substrate recognition.

According to the results of Ca^{2+}-dependent enzymatic activity assays, binding of Ca^{2+} to a phytase increases catalytic activity by neutralizing the negatively charged cleft (Ha et al., 2000). Likewise, the active site cleft of LysB4 is largely decorated by the acidic residues (Glu54, Asp87, Asp129, Glu134, and Asp137; Fig. 3C). We suggest that Zn^{2+} or other divalent ions might mediate the ionic interaction to *meso*-DAP by binding to the negatively charged residues of LysB4, although further study might be needed. In conclusion, our high resolution structure of the LysB4 protein provides insight into the molecular mechanism of how endolysins in bacteriophages recognize and hydrolyze the host peptidoglycans.

Note: Supplementary information is available on the Molecules and Cells website (www.molcells.org).

ACKNOWLEDGMENTS

This research was supported by National Research Foundation of Korea (NRF-2017H1A2A1042661-Global Ph.D. Fellowship Program to SH), Korea Institute of Planning and Evaluation for Technology in Food, Agriculture, Forestry (IPET) through Agriculture, Food and Rural Affairs Research Center Support Program, funded by Ministry of Agriculture, Food and Rural Affairs (MAFRA) (710012-03-1-HD120 to NCH), and National Research Foundation of Korea grant funded by the Korea government (MSIP) (No. NRF-2017R1A2A1A17069378 to SR). We made use of beamline 5C and 7A at Pohang Accelerator Laboratory (Pohang, Republic of Korea).

REFERENCES

Adams, P.D., Afonine, P.V., Bunkoczi, G., Chen, V.B., Davis, I.W., Echols, N., Headd, J.J., Hung, L.W., Kapral, G.J., Grosse-Kunstleve, R.W., et al. (2010). PHENIX: a comprehensive Python-based system

for macromolecular structure solution. Acta Crystallogr. D. Biol. Crystallogr. *66*, 213-221.

Asensio, J.L., Arda, A., Canada, F.J., and Jimenez-Barbero, J. (2013). Carbohydrate-aromatic interactions. Acc. Chem. Res. *46*, 946-954.

Bochtler, M., Odintsov, S.G., Marcyjaniak, M., and Sabala, I. (2004). Similar active sites in lysostaphins and D-Ala-D-Ala metallopeptidases. Protein Sci. *13*, 854-861.

Borysowski, J., Weber-Dąbrowska, B., and Górski, A. (2006). Bacteriophage endolysins as a novel class of antibacterial agents. Exp. Biol. Med. *231*, 366-377.

Bussiere, D.E., Pratt, S.D., Katz, L., Severin, J.M., Holzman, T., and Park, C.H. (1998). The structure of VanX reveals a novel amino-dipeptidase involved in mediating transposon-based vancomycin resistance. Mol. Cell *2*, 75-84.

Dziarski, R., and Gupta, D. (2006). The peptidoglycan recognition proteins (PGRPs). Genome Biol. *7*, 232.

Emsley, P., Lohkamp, B., Scott, W.G., and Cowtan, K. (2010). Features and development of Coot. Acta Crystallogr. D. Biol. Crystallogr. *66*, 486-501.

Etobayeva, I., Linden, S.B., Alem, F., Harb, L., Rizkalla, L., Mosier, P.D., Johnson, A.A., Temple, L., Hakami, R.M., and Nelson, D.C. (2018). Discovery and Biochemical Characterization of PlyP56, PlyN74, and PlyTB40—*Bacillus* Specific Endolysins. Viruses *10*, 276.

Fukushima, T., Yao, Y., Kitajima, T., Yamamoto, H., and Sekiguchi, J. (2007). Characterization of new L, D-endopeptidase gene product CwlK (previous YcdD) that hydrolyzes peptidoglycan in *Bacillus subtilis*. Mol. Genet. Genomics *278*, 371-383.

Ha, N.C., Oh, B.C., Shin, S., Kim, H.J., Oh, T.K., Kim, Y.O., Choi, K.Y., and Oh, B.H. (2000). Crystal structures of a novel, thermostable phytase in partially and fully calcium-loaded states. Nat. Struct. Biol. *7*, 147-153.

Jang, Y., Choi, G., Hong, S., Jo, I., Ahn, J., Choi, S.H., and Ha, N.C. (2018). A Novel Tetrameric Assembly Configuration in VV2_1132, a LysR-Type Transcriptional Regulator in Vibrio vulnificus. Mol. Cells *41*, 301-310.

Jones, P., Binns, D., Chang, H.Y., Fraser, M., Li, W., McAnulla, C., McWilliam, H., Maslen, J., Mitchell, A., Nuka, G., et al. (2014). InterProScan 5: genome-scale protein function classification. Bioinformatics *30*, 1236-1240.

Kamisango, K., Saiki, I., Tanio, Y., Okumura, H., Araki, Y., Sekikawa, I., Azuma, I., and Yamamura, Y. (1982). Structures and biological activities of peptidoglycans of Listeria monocytogenes and Propionibacterium acnes. J. Biochem. *92*, 23-33.

Korndorfer, I.P., Kanitz, A., Danzer, J., Zimmer, M., Loessner, M.J., and Skerra, A. (2008). Structural analysis of the L-alanoyl-D-glutamate endopeptidase domain of Listeria bacteriophage endolysin Ply500 reveals a new member of the LAS peptidase family. Acta Crystallogr. D. Biol. Crystallogr. *64*, 644-650.

Lee, J.H., Shin, H., Son, B., Heu, S., and Ryu, S. (2013). Characterization and complete genome sequence of a virulent bacteriophage B4 infecting food-borne pathogenic *Bacillus cereus*. Arch. Virol. *158*, 2101-2108.

Leive, L. (1968). Studies on the permeability change produced in coliform bacteria by ethylenediaminetetraacetate. J. Biol. Chem. *243*, 2373-2380.

Lim, J.H., Kim, M.S., Kim, H.E., Yano, T., Oshima, Y., Aggarwal, K., Goldman, W.E., Silverman, N., Kurata, S., and Oh, B.H. (2006). Structural basis for preferential recognition of diaminopimelic acid-type peptidoglycan by a subset of peptidoglycan recognition proteins. J. Biol. Chem. *281*, 8286-8295.

Loessner, M.J. (2005). Bacteriophage endolysins—current state of research and applications. Curr. Opin. Microbiol. *8*, 480-487.

Loessner, M.J., Wendlinger, G., and Scherer, S. (1995). Heterogeneous endolysins in Listeria monocytogenes bacteriophages: a new class of enzymes and evidence for conserved holin genes within the siphoviral lysis cassettes. Mol. Microbiol. *16*, 1231-1241.

McCafferty, D.G., Lessard, I.A., and Walsh, C.T. (1997). Mutational analysis of potential zinc-binding residues in the active site of the enterococcal D-Ala-D-Ala dipeptidase VanX. Biochem. *36*, 10498-10505.

McCoy, A.J., Grosse-Kunstleve, R.W., Adams, P.D., Winn, M.D., Storoni, L.C., and Read, R.J. (2007). Phaser crystallographic software. J. Appl. Crystallogr. *40*, 658-674.

Nelson, D.C., Schmelcher, M., Rodriguez-Rubio, L., Klumpp, J., Pritchard, D.G., Dong, S., and Donovan, D.M. (2012). Endolysins as antimicrobials. In Adv. Virus Res. (Elsevier), pp. 299-365.

Nelson, M.D., and Fitch, D.H. (2012). Overlap extension PCR: an efficient method for transgene construction. In Molecular Methods for Evolutionary Genetics (Springer), pp. 459-470.

Otwinowski, Z., and Minor, W. (1997). Processing of X-ray diffraction data collected in oscillation mode. Methods Enzymol. *276*, 307-326.

Owen, R.A., Fyfe, P.K., Lodge, A., Biboy, J., Vollmer, W., Hunter, W.N., and Sargent, F. (2018). Structure and activity of ChiX: a peptidoglycan hydrolase required for chitinase secretion by Serratia marcescens. Biochem. J. *475*, 415-428.

Schleifer, K.H., and Kandler, O. (1972). Peptidoglycan types of bacterial cell walls and their taxonomic implications. Bacteriol. Rev. *36*, 407-477.

Schmelcher, M., Donovan, D.M., and Loessner, M.J. (2012). Bacteriophage endolysins as novel antimicrobials. Future Microbiol. *7*, 1147-1171.

Son, B., Yun, J., Lim, J.A., Shin, H., Heu, S., and Ryu, S. (2012). Characterization of LysB4, an endolysin from the *Bacillus cereus*-infecting bacteriophage B4. BMC Microbiol. *12*, 33.

Vagin, A., and Teplyakov, A. (2010). Molecular replacement with MOLREP. Acta Crystallogr. D. Biol. Crystallogr. *66*, 22-25.

Vollmer, W., Blanot, D., and de Pedro, M.A. (2008). Peptidoglycan structure and architecture. FEMS Microbiol. Rev. *32*, 149-167.

Winn, M.D., Ballard, C.C., Cowtan, K.D., Dodson, E.J., Emsley, P., Evans, P.R., Keegan, R.M., Krissinel, E.B., Leslie, A.G., McCoy, A., et al. (2011). Overview of the CCP4 suite and current developments. Acta Crystallogr. D. Biol. Crystallogr. *67*, 235-242.